"REAL TIME" DETERMINATION OF POROSITY DEVELOPMENT IN CARBONS: A COMBINED SAXS/TGA APPROACH

J.M. Calo[*], P.J. Hall[†], S. Houtmann[†], R.E. Winans[‡], and Soenke Seifert[‡]
[*]Division of Engineering, Brown University, Providence, RI, USA
[†]Department of Chemical Engineering, Strathclyde University, Glasgow, Scotland, UK
[‡]Chemistry Division & APS/BESSRC-CAT, Argonne National Laboratory, Argonne, IL, USA

Introduction

Small angle scattering (SAS) techniques offer a number of advantages for the investigation of the nature and behavior of porous materials. In particular, with respect to carbons, the nonintrusive nature of SAS means that, in principle, characterization can be performed on carbons *in situ* during activation/gasification processes, allowing real time resolution of porosity development. These types of studies have not been practical nor possible heretofore, primarily due to the prohibitively long counting times required to span the requisite wave vector (q) range over the entire burn-off process. However, the availability of new instruments, such as the small angle X-ray scattering (SAXS) facility at the Advanced Photon Source (APS) at the Argonne National Laboratory (ANL), has now made these types of experiments possible. Some of the preliminary data from these efforts have been reported previously [1], and here we present selected results incorporating a thermogravimetric analyzer in the experimental system to measure burn-off simultaneously with the collection of small angle X-ray scattering (SAXS) data.

Experimental

The SAXS instrument was constructed at ANL and used on the Basic Energy Sciences Synchrotron Radiation Center (BESSRC-CAT) undulator beamline ID-12 at the APS. Monochromatic X-rays (8.98 keV here) were scattered off the samples and collected on a 19 x 19 cm^2, position-sensitive, two-dimensional gas detector array. The scattered intensities were corrected for absorption, empty cell scattering, and instrument background.

A Cahn TG-121 thermogravimetric apparatus (TGA) was adapted for use directly in the beamline. Two holes, approximately 2 cm in diameter, located 180° apart, were drilled through the walls of the TGA furnace to accommodate the X-ray beam. Two corresponding holes were also made in the quartz hangdown tube of the TGA to admit the X-ray beam. A photograph of the resultant arrangement is presented in Figure 1.

Char samples, on the order of tens of mg, contained in aluminum foil packets with multiple perforations (to allow for adequate transport of oxygen through the sample), were suspended from the microbalance on a platinum wire.

The experimental arrangement and procedures were gradually improved with increasing experience with the system. Two problems were of particular note. Since the TGA system was operated in an "open" mode, the reaction gas (oxygen) was used to purge the quartz hangdown tube to maintain uniform composition and temperature. With the flow rate set too high, the sample tended to oscillate back and forth on the platinum wire. This resulted in some observable oscillation in scattering intensity at high time resolutions. This problem was solved by simply lowering the oxygen flow rate to the point where sample oscillation vanished. Another problem was associated with the location of the sample thermocouple, as necessitated by the experimental arrangement. This resulted in a systematic offset in the temperature measurements from the actual sample temperature. This problem was rectified *via* calibrations of the sample temperature in a laboratory TGA.

10 g samples of saran and microgranular cellulose, obtained from the Aldrich Chemical Co., were heated in a tube furnace at 10K/min to 900°C, with a 1h heat soak time, under flowing nitrogen. Calcium-loaded cellulose was prepared by mixing with calcium acetate solution, followed by drying. The resultant calcium content was approximately 3% following carbonization.

Results

Saran Char. The TGA data presented in Figure 2 were obtained under nonisothermal conditions in an atmosphere of oxygen. As shown, the sample was first rapidly heated to 200°C, held at that temperature for 2 min, and then heated to 560°C at 6K/min, followed by an isothermal period at the final temperature. It appears that the bulk of the sample burnt out at about 52 min, prior to attaining the final temperature. From this point

on, the mass signal appears to be due to slow burnout of residual, presumably more unreactive, material.

SAXS curves corresponding to selected points during the activation history of the sample are presented in Figure 3. In the absence of other effects, scattering at high wave vector (q) values is primarily due to microporosity, while that in the low range is due to meso- and larger porosity [2].

In Figure 3, the plateau at high q early in the activation history is indicative of a significant level of initial microporosity. At low-burn-offs there is a considerable decrease in the mesoporosity, accompanied by microporosity development at high q. The latter continues up to about 49 minutes into the activation regimen. Thereafter, scattering in the microporosity region falls off rapidly as the carbon in the micropores is burned off. The considerable drop-off in scattering intensities over the entire q range at high burn-offs is consistent with pore wall collapse over a wide range of pore sizes.

Somewhat similar results were obtained for saran char under near-isothermal conditions in oxygen. As shown in Figure 4, the sample temperature for this experiment was increased at 60K/min to 435°C and held there. As indicated, the sample mass actually began to decrease prior to attaining the isothermal portion of the program..

Representative SAXS curves in the low burn-off regime are presented in Figure 5. As shown, the predominant behavior is net microporosity development at high q proceeding from light to darker orange, while scattering from the larger pores remains relatively constant. The last curve (red) in that plot actually shows a net decrease in the microporosity.

SAXS data at higher burn-offs during activation of the same sample are presented in Figure 6. From red-to-orange-to-yellow-to-green, the predominant behavior is net consumption of mesoporosity, while the net microporosity remains relatively constant. From green-to-blue there appears to be a "transition" where the porosity decreases significantly over the entire q-range. Following that, however, the lavender curve indicates an *increase* in net mesoporosity at the expense of microporosity. The gray curve then shows another significant decrease over the entire q-range. This is followed by another similar decrease to the black curve. But then from black-to-gold there is another region of significant microporosity decrease while maintaining relatively constant net mesoporosity.

These data suggest a dynamic porosity development mechanism. Starting with the original sample, it begins with microporosity production leading to net microporosity loss (*cf.* Figure 5), with little net change in the larger porosity. It then appears to progress through periods of net porosity variations that are alternately focused in the mesoporosity and then in the microporosity, with transitional periods over which the net changes gradually involve a broader range of pore sizes. Of course, only *net* porosity differences are observed. Thus when the porosity in one particular size range is relatively constant, this could be due either to no appreciable reaction occurring in those pores at that particular stage in the activation, or that the rates of consumption and development are in relative balance over this burn-off range. Since it would be difficult to reconcile the former mechanism with the nature of the activation process, it appears that the *net population balance* of pores in a particular size range is responsible for these observations. This interpretation is supported by data such as the lavender curve in Figure 6 where the net mesoporosity actually increases, while the net microporosity decreases. Apparently, the *rate* of mesoporosity development exceeded that of consumption at that point in the activation history.

Cellulose Char. TGA data for a cellulose char sample are presented in Figure 7. As shown, in this experiment the char was activated isothermally at 425°C.

Selected scattering curves over the sample activation history are presented in Figure 8. These data indicate that this carbon, like the saran char, initially exhibits a significant amount of microporosity, as indicated by the plateau centered at about $q = 0.1Å^{-1}$. However, the behavior of this microporosity with activation is somewhat different. As shown, initially the microporosity increases much more markedly than in the saran char. This aspect is even more evident in Figure 9 that presents the same data on a linear scale, recast as scattering intensity differences relative to the initial scattering curve. Microporosity development occurs along with some loss of the smallest pores at the highest q values, and also the larger pores at the lowest q values. In the vicinity of 40-50% burn-off, the net development of microporosity gives way to net consumption. Progressive activation beyond this point causes a continual, monotonic decrease in the scattering intensity over the entire q range.

Differences in the behavior of the microporosity in the saran and cellulose chars may be related to "closed porosity." It is well known that "glassy" carbons can exhibit a considerable amount of microporosity that is initially "blocked" from access to the activating agent by amorphous carbon. Early activation of these types of carbons primarily involves preferential burn-off of the amorphous carbon, exposing the intrinsic underlying

microporous structure. For example, using contrast-matching small angle neutron scattering, no new microporosity development was observed upon activation of a char produced from a highly crosslinked phenol-formaldehyde resin up to 21% burn-off [2]. The only mechanism observed was burn-off of amorphous carbon and unblocking of initially "closed" microporosity. Unfortunately, SAXS is not amenable to contrast-matching as is SANS. Consequently, this approach could not be used in the current experiments. However, it is suspected that this may be the reason that the evolution of microporosity with activation is much slower and less marked in the saran char than in the cellulose char.

Calcium-Loaded Cellulose Char. TGA data for the Ca-loaded char are unavailable since these data were obtained prior to the TGA being incorporated into the experimental system. A 1 mm diameter quartz capillary was used as the sample holder.

As shown in Figure 10, the behavior of the Ca-loaded cellulose char is considerably different than that of the unpromoted cellulose (as in Figure 8). Most notably, the early activation history is marked by *increasing* scattering intensities with burn-off at low q values. These same data are presented as difference curves with respect to the initial scattering curve in Figure 11 in order to accentuate this behavior on a linear scale. As shown, at 50 min the difference curve is *positive* at low q, and then decreases to zero with increasing q. By 100 min the entire difference curve has become *negative;* i.e., scattering has *decreased* with respect to the initial material. This behavior is similar to that observed for phenolic resin char at low q at low burn-offs, that was attributed primarily to preferential gasification of amorphous carbon clusters of characteristically large sizes [2]. By 200 min, the curve is still negative at low q, but becomes positive again at higher q, proceeds through a maximum at about 0.08 $Å^{-1}$, and then falls to zero again. The evolution of this same pattern continues with burn-off, with the maximum increasing in intensity, while progressively shifting to lower q. The negative difference curves eventually disappear due to the counteracting effect of porosity development, that progressively increases scattering from smaller pores at high q to larger pores at low q. At very high burn-offs, scattering intensity increases markedly at low q due to the production of large pores as a result of pore wall collapse. As shown, there appears to be little microporosity development in the high q range over the entire activation history. The preferential development of mesoporosity rather than microporosity in the Ca-loaded char may be due to the catalytic effect of calcium, which may not have been well dispersed in the smallest pores.

Conclusions

The SAXS/TGA approach has been demonstrated to be a useful technique for time-resolution of porosity development in carbons during activation processes. Qualitative interpretation of the data obtained thus far suggests that a population balance approach focusing on the rates of production and consumption of pores as a function of size may be a fruitful approach to the development of quantitative models of activation processes. These then could become useful tools for the optimization of pore size distributions for particular applications by providing descriptions and predictions of how various activating agents and time-temperature histories affect resultant pore size distributions.

References

1. Calo, J.M., Hall, P.J., Brown, S.D., Winans, R.E., and Seifert, S. Real time determination of porosity development in carbons using SAXS. Proc. Eurocarbon 2000; Berlin, Germany, 113-114.
2. Antxustegi, M.M., Hall, P.J., and Calo, J.M. The use of contrast-matching small-angle neutron scattering techniques to monitor closed porosity in carbons. J. Coll. Intf. Sci. 1998; 202, 490-498.

Acknowledgements

The authors acknowledge EPSRC support under grant number GR/N03006. Use of the Advanced Photon Source was supported by the U.S. Department of Energy, Basic Energy Sciences, Office of Energy Research, under Contract No. W-31-109-ENG-38.

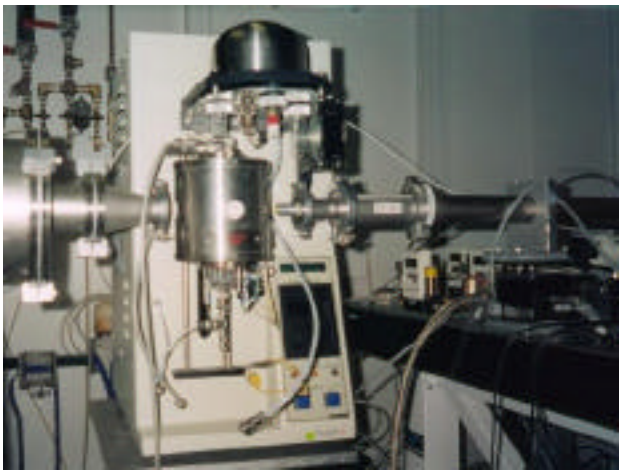

Figure 1. Photograph of the Cahn TG-121 thermogravimetric analyzer installed in the BESSRC-CAT beamline ID-12 at the Advanced Photon Source at the Argonne National Laboratory, Argonne, Illinois; November, 2000.

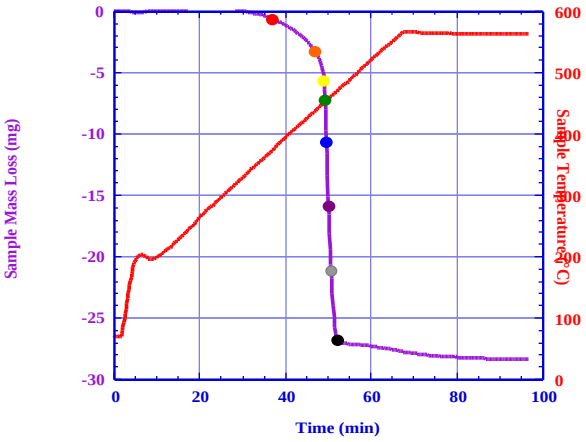

Figure 2. Saran char TGA data during nonisothermal activation in oxygen. The color-coded data points correspond to the SAXS curves presented in Figure 3.

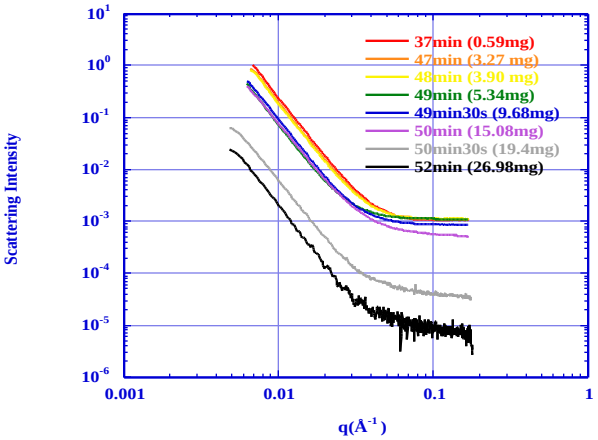

Figure 3. SAXS curves for saran char activated in oxygen to the indicated mass losses. The color-coded curves correspond to the points in Figure 2 on the mass loss curve.

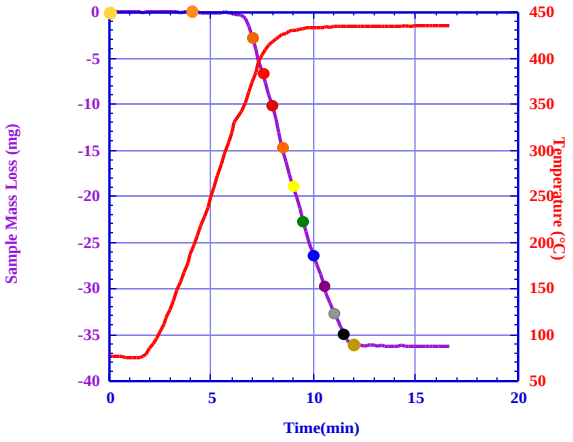

Figure 4. Saran char TGA data during near-isothermal activation in oxygen at 435°C. The color-coded data points correspond to the SAXS curves presented in Figures 5 and 6.

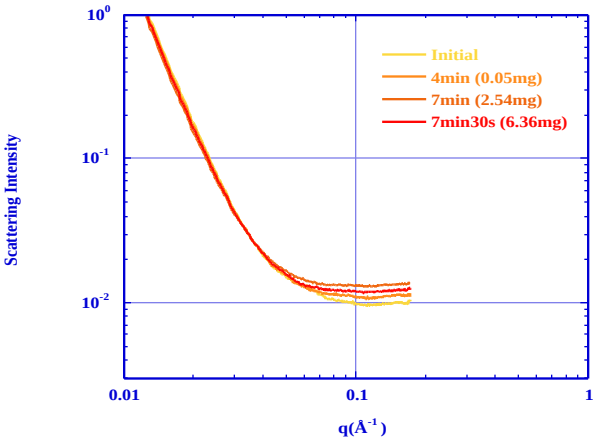

Figure 5. SAXS curves for saran char activated in oxygen at 435°C to the indicated mass loss in the low burn-off regime. The color-coded curves correspond to the points in Figure 4 on the mass loss curve.

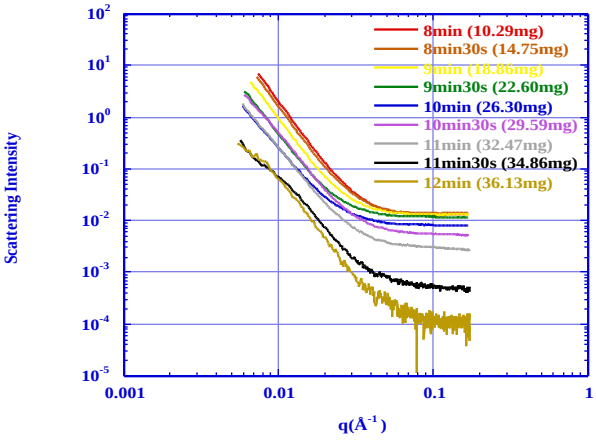

Figure 6. SAXS curves for saran char activated in oxygen at 435°C to the indicated mass losses in the high burn-off regime. The color-coded curves correspond to the points in Figure 4 on the mass loss curve.

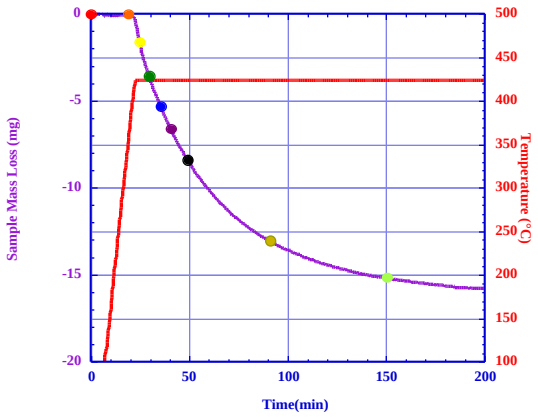

Figure 7. TGA data for cellulose char during isothermal activation in oxygen at 425°C. The color-coded data points correspond to the SAXS curves presented in Figure 8.

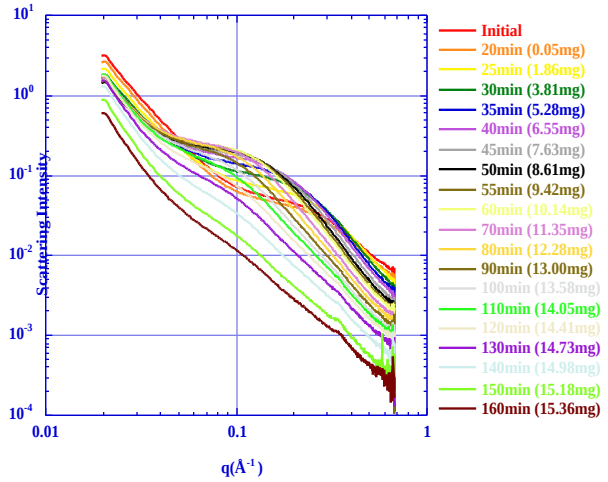

Figure 8. SAXS curves for cellulose char during isothermal activation in oxygen to the mass losses indicated.

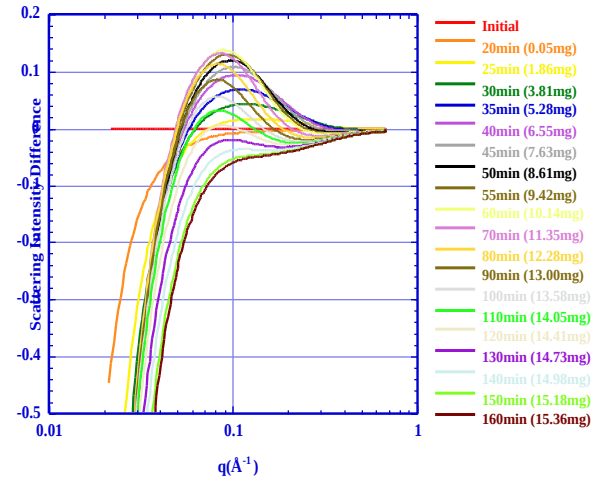

Figure 9. Scattering intensity *differences* from the SAXS curve of the initial sample (i.e., t = 0) as a function of time for the data in Figure 8.

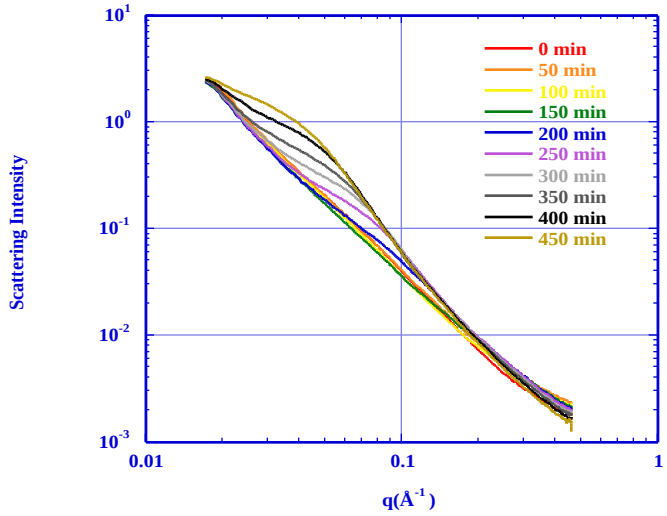

Figure 10. SAXS curves for Ca-loaded cellulose char during isothermal activation at 340°C in oxygen as a function of time. The total burn-off was 73%.

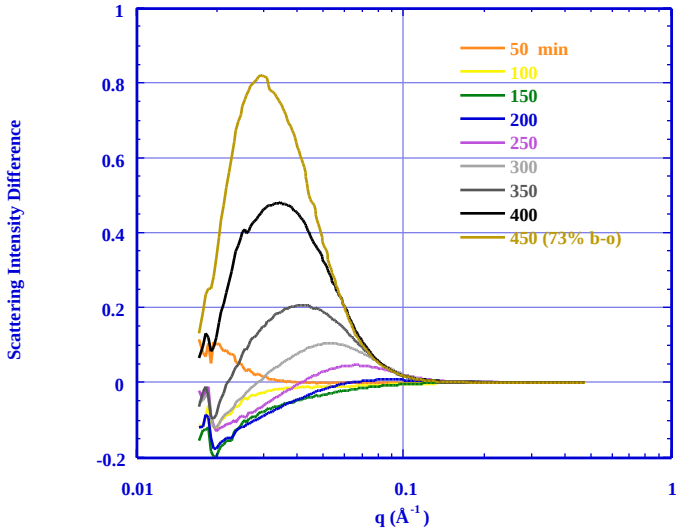

Figure 11. Scattering intensity *differences* from the SAXS curve of the initial sample (i.e., t = 0) as a function of time for the data in Figure 10.